Optics Letters

# Frequency-doubling of continuous laser light in the Laguerre–Gaussian modes $LG_{0,0}$ and $LG_{3,3}$

Joscha Heinze,* Henning Vahlbruch, and Benno Willke

*Max-Planck-Institut für Gravitationsphysik (Albert-Einstein-Institut) and Leibniz Universität Hannover, 30167 Hannover, Germany*
**Corresponding author: joscha.heinze@aei.mpg.de*

*Received 9 July 2020; accepted 7 August 2020; posted 12 August 2020 (Doc. ID 402371); published 14 September 2020*

**For future generations of gravitational wave detectors, it is proposed to use the helical Laguerre–Gaussian $LG_{3,3}$ mode to reduce thermal noise, which limits the detector sensitivity. At the same time, this requires the efficient generation of squeezed vacuum states in the $LG_{3,3}$ mode for quantum noise reduction. Since this technique includes the process of second harmonic generation (SHG), we experimentally compare the conversion efficiency and harmonic output field of the $LG_{0,0}$ and $LG_{3,3}$ modes in a cavity-enhanced SHG using the same 7% doped MgO:$LiNbO_3$ crystal. Conversion efficiencies of 96% and 45% are achieved, respectively. The influence of mode mismatches and astigmatism is analyzed to estimate the ratio of the pump mode-dependent effective nonlinearities to be $d_{0,0}/d_{3,3} \sim 5$. Furthermore, we show that absorption loss in the crystal is more relevant for the $LG_{3,3}$ mode.** 

https://doi.org/10.1364/OL.402371



One of the fundamental noise sources in second generation gravitational wave detectors such as Advanced LIGO and Advanced Virgo, besides, e.g., quantum and seismic noise, is coating Browning thermal noise, which limits the sensitivity of these detectors in the highly interesting frequency range around 100 Hz [1,2]. Instead of the currently used fundamental Gaussian mode, higher-order Laguerre–Gauss (LG) modes have been proposed as one method to reduce the coupling of this thermal noise to the sensitivity of future detector generations [3]. Several experiments have already demonstrated the high-purity generation of the helical $LG_{3,3}$ mode and its general compatibility with the design of gravitational-wave detectors [4–8]. However, challenges with respect to mode degeneracy have also been reported [9,10]. One remaining question is whether squeezed vacuum states, injected into the detectors to reduce quantum noise [11], can be efficiently generated in the $LG_{3,3}$ mode. The most mature approach to produce continuous-wave squeezed vacuum states in the fundamental $LG_{0,0}$ mode uses second harmonic generation (SHG) and subsequent parametric down-conversion [12,13]. To gain first insights into the transferability of this method to the $LG_{3,3}$ mode, we analyze its conversion efficiency, harmonic output field, and absorption losses in a continuously pumped, cavity-enhanced SHG in comparison to the $LG_{0,0}$ mode.

In general, the intensity of higher-order modes is distributed more uniformly over a larger transverse area compared to the fundamental mode of the same beam radius. This implies lower peak intensities, which reduces the interaction with a nonlinear crystal. Assuming identical Gaussian beam parameters (waist size and waist position), a beam in the $LG_{3,3}$ mode (mode order $\sigma = 9$) thus requires more power to achieve the same conversion efficiency as a beam in the $LG_{0,0}$ mode (mode order $\sigma = 0$). We present an experimental investigation of this fundamental difference and quantify it via a pump mode-dependent effective nonlinearity $d_{p,l}$ of the nonlinear medium [14]. Mode mismatches and astigmatism at the SHG cavity, however, reduce the resonant power such that the measured efficiency is lower than the theoretical limit. Hence, three types of efficiencies are presented: the *external* conversion efficiency $\eta_{\mathrm{ext}} = P_{\mathrm{out}}/P_{\mathrm{in}}^{\mathrm{ext}}$ refers to the ratio of the harmonic output power $P_{\mathrm{out}}$ to the fundamental input power $P_{\mathrm{in}}^{\mathrm{ext}}$, which is sent to the SHG cavity. The *corrected* conversion efficiency $\eta_{\mathrm{cor}} = P_{\mathrm{out}}/P_{\mathrm{in}}^{\mathrm{mat}}$ with $P_{\mathrm{in}}^{\mathrm{mat}} = P_{\mathrm{in}}^{\mathrm{ext}}|\kappa|^2$ takes a non-ideal mode matching of the input beam to the SHG cavity and effects due to astigmatism via the power coupling coefficient $|\kappa|^2$ into account. The experimental data is then compared to simulation results computed with the nonlinear cavity simulator (NLCS) [15]. This comparison allows us to estimate the effective nonlinearity $d_{p,l}$ of the used medium and the medium-independent ratio $d_{0,0}/d_{3,3}$ for the used beam focusing parameter. Finally, the *effective* conversion efficiency $\eta_{\mathrm{eff}} = P_{\mathrm{out}}^{\mathrm{eff}}/P_{\mathrm{in}}^{\mathrm{ext}}$ includes the output mode purity $\mu_{\mathrm{out}}$, where $P_{\mathrm{out}}^{\mathrm{eff}} = P_{\mathrm{out}}\mu_{\mathrm{out}}$ is the fraction of the harmonic output power, which is in a pure spatial mode.

Cavity-enhanced nonlinear processes are prone to non-cylindrically symmetric abberations like astigmatism due to imperfect cavity mirrors and inhomogeneities in the nonlinear crystal. Here, we use a simplified model of an astigmatic cavity to illustrate how this influences the SHG. Additional distortion of the resonant modes or scattering into other modes (see, e.g., [16,17]) are neglected. The model considers a linear cavity with a plane mirror (radius of curvature $R_{c1} = \infty$) and a mirror that features two different radii of curvature $R_{c2,x}$ and $R_{c2,y}$ on the $x$ and $y$ axis, respectively ($z$ defines the optical axis in this case). This astigmatism breaks the cylindrical symmetry and the cavity now favors the rectangularly symmetric Hermite–Gaussian (HG) modes over the cylindrically symmetric LG modes. The $LG_{3,3}$ mode will thus be decomposed as [5]

$$\mathrm{LG}_{3,3} = \sum_{k=0}^{9} c_{k,9-k}\mathrm{HG}_{k,9-k} \quad \text{with} \quad \sum_{k=0}^{9} \left|c_{k,9-k}\right|^2 = 1, \tag{1}$$

where $c_{k,9-k}$ are complex coefficients. Each of these $\mathrm{HG}_{m,n}$ modes is assumed to see an individual effective radius of curvature $R_{c2}$ at the curved mirror, defined as

$$R_{c2}(m,\, n) := \frac{m R_{c2,x} + n R_{c2,y}}{\sigma}, \tag{2}$$

because the mode indices $m$ and $n$ quantify how the intensity of $\mathrm{HG}_{m,n}$ is distributed between the $x$ and $y$ axis. Since the round-trip Gouy phase $\xi^{\mathrm{rt}}$ in this cavity is given by [18]

$$\xi^{\mathrm{rt}}_{m,n} = 2\arccos(\mathrm{sign}(g_1) \times \sqrt{g_1 g_2(m,\, n)}), \tag{3}$$

where $g_1 = 1 - L/R_{c1}$ and $g_2(m,\, n) = 1 - L/R_{c2}(m,\, n)$ with the cavity length $L$, the HG modes are not resonant for the same cavity length anymore and are separated in the normalized resonance/transmission spectrum according to [19]

$$P_{\mathrm{res}}(L) = \sum_{k=0}^{9} \frac{P_{k,9-k}}{1 + \left(\frac{2\mathcal{F}}{\pi}\right)^2 \sin^2\left(\frac{-\pi L}{\lambda} + 5\xi^{\mathrm{rt}}_{k,9-k}\right)}, \tag{4}$$

where $P_{k,9-k} = |c_{k,9-k}|^2$, $\mathcal{F}$ is the finesse, and $\lambda$ is the wavelength (see Fig. 1).

In an experiment, the cavity length is typically stabilized to the resonance condition of the mode of interest or, more generally, to the maximum of $P_{\mathrm{res}}(L)$, which will be referred to as "in lock." In the case of astigmatism, the maximum of $P_{\mathrm{res}}(L)$ does not coincide with the individual maxima of the HG resonances anymore. In lock, each HG mode therefore sees a different power buildup such that the circulating mode composition deviates from a pure $\mathrm{LG}_{3,3}$ mode. This will affect the output mode purity and cause mode mismatches between the injected and resonating field in addition to deviating waist sizes and positions. The latter effect reduces the effective mode matching to the SHG cavity and, thereby, the circulating power.

Due to the astigmatism and additional mode distortion, the cavity eigenfield in lock will not resemble a pure LG mode. Furthermore, the injected field is typically not in a pure mode either and may have slightly different Gaussian beam parameters than the cavity eigenfield. Both effects lead to an imperfect overlap of the injected and eigenfield and to some input power being reflected even off an impedance-matched cavity. The matched fraction of the input power can be quantified by the absolute value squared of the overlap integral between the injected field and eigenfield $|\kappa|^2$ and called matched input power $P_{\mathrm{in}}^{\mathrm{mat}}$.

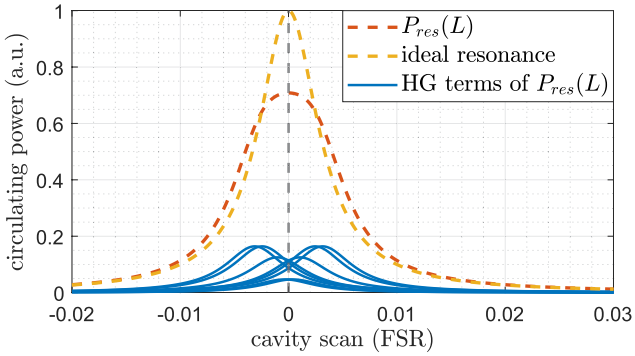


**Fig. 1.** Simulated circulating power in an astigmatic cavity for an injected $\mathrm{LG}_{3,3}$ mode using $\mathcal{F} = 300$, $R_{c2,x} = 0.5000$ m, $R_{c2,y} = 0.5012$ m, and $L = 21$ cm. FSR is the free spectral range, *ideal resonance* assumes no astigmatism.

For the $\mathrm{LG}_{0,0}$ mode, we could neglect astigmatism, as the generated harmonic $\mathrm{LG}_{0,0}$ mode showed no measurable deviation from the $\mathrm{LG}_{0,0}$ eigenmode of a subsequent triangular reference cavity. The mode matching of the fundamental beam to the SHG cavity was inferred from the higher-order mode analysis of the transmission spectrum of the SHG cavity.

In the $\mathrm{LG}_{3,3}$ case, the transmission spectrum of the SHG cavity could not be used to infer the effective mode matching. Especially at higher levels of input power, the resonances, which are ideally shaped like in Fig. 1, were deformed by astigmatism such that the higher-order mode content could not be properly analyzed. Instead, the reflected fundamental power, the transmitted fundamental power, and the harmonic output power were measured and inserted into the corresponding steady-state equations of the SHG cavity. This set of three equations includes $|\kappa|^2$ as well as the single-pass power absorption coefficient $l^a$ of the fundamental field and the single-pass power conversion coefficient $c$ as unknown parameters:

$$\begin{aligned} r_{\mathrm{refl}} &:= P_{\mathrm{refl}}/P_{\mathrm{in}}^{\mathrm{ext}} = 1 - \gamma|\kappa|^2 = 1 - \left[1 - \left|a_{\mathrm{refl}}(l^a,\, c)\right|^2\right]|\kappa|^2, \\ r_{\mathrm{trans}} &:= P_{\mathrm{trans}}/P_{\mathrm{in}}^{\mathrm{ext}} = |a_{\mathrm{trans}}(l^a,\, c)|^2|\kappa|^2, \\ \eta_{\mathrm{ext}} &:= P_{\mathrm{out}}/P_{\mathrm{in}}^{\mathrm{ext}} = |b_{\mathrm{out}}(l^a,\, c)|^2|\kappa|^2, \end{aligned} \tag{5}$$

with

$$\begin{aligned} a_{\mathrm{refl}}(l^a,\, c) &= \rho_1^a - \frac{(\tau_1^a)^2(\tau_{\mathrm{AR}}^a)^2\rho_2^a(1 - l^a - c)}{1 - \rho_1^a\rho_2^a(\tau_{\mathrm{AR}}^a)^2(1 - l^a - c)}, \\ a_{\mathrm{trans}}(l^a,\, c) &= -\frac{\tau_1^a\tau_2^a\tau_{\mathrm{AR}}^a\sqrt{1 - l^a - c}}{1 - \rho_1^a\rho_2^a(\tau_{\mathrm{AR}}^a)^2(1 - l^a - c)}, \\ b_{\mathrm{out}}(l^a,\, c) &= -\frac{\tau_1^a\tau_{\mathrm{AR}}^a\tau_{\mathrm{AR}}^b\sqrt{c((\rho_2^b)^2 + (1 - l^a - c)(\rho_2^a)^2)}}{1 - \rho_1^a\rho_2^a(\tau_{\mathrm{AR}}^a)^2(1 - l^a - c)}, \end{aligned} \tag{6}$$

where $\gamma$ is the power reflection coefficient due to the impedance condition, and the other parameters are allocated in Fig. 2; $\rho$ and $\tau$ are amplitude reflection and transmission coefficients, respectively; 1, 2, and AR indicate the incoupling mirror, crystal end face, and anti-reflection-coated face, respectively; $a$ and $b$ indicate the fundamental and harmonic field, respectively. The absorption of the harmonic field is neglected, and the absorption and conversion of the fundamental field are assumed to be equal for both passes through the crystal during one roundtrip

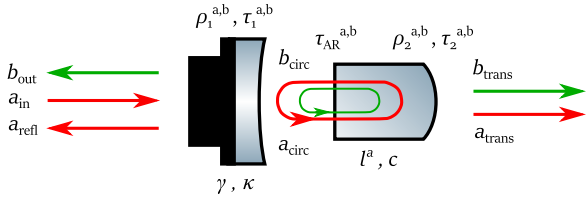


**Fig. 2.** The hemilithic SHG cavity is formed by an incoupling mirror and the curved crystal face. This figure allocates all relevant fields and cavity properties used in Eq. (5).

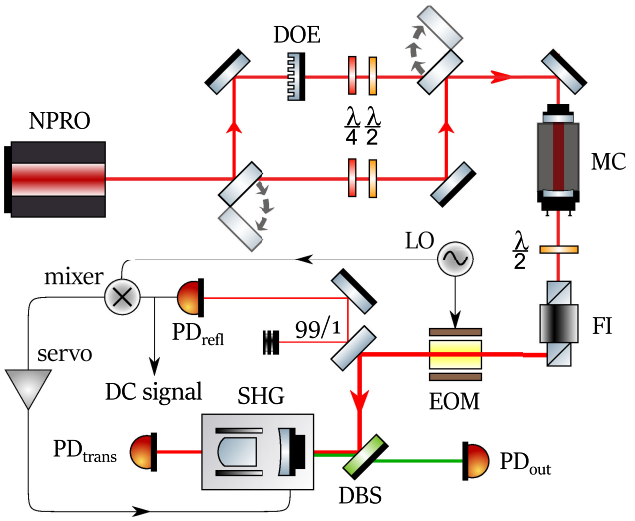


**Fig. 3.** Schematic of experimental setup. Not shown: FI right after the laser and the PDH locking scheme of the MC.

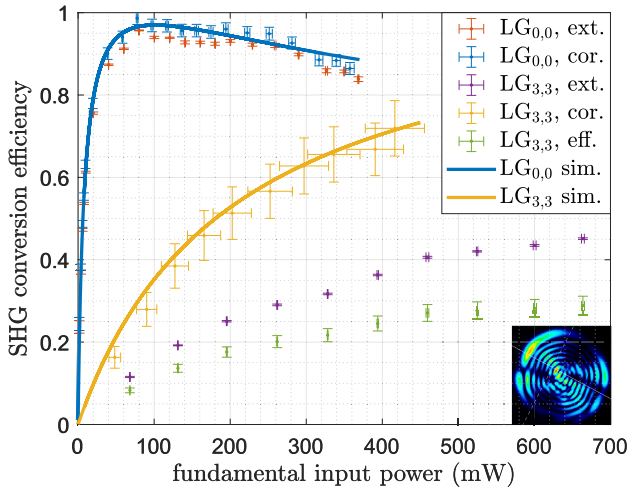


**Fig. 4.** Measured external, corrected, and effective SHG conversion efficiencies of the $LG_{0,0}$ and $LG_{3,3}$ modes, including the NLCS simulations for the corrected curves. The $x$ axis refers to the full input power for the external and effective efficiencies and to the estimated matched input power for the corrected and simulated efficiencies. Bottom right: CCD picture of the harmonic output field at $P_{in}^{ext} = 664$ mW for the $LG_{3,3}$ mode. A distorted $LG_{6,6}$ intensity pattern can be identified.

because the fundamental field is nearly undepleted after the first pass.

The uncertainty in the nominal $\rho_2^a$ had a very high impact on the result for $|\kappa|^2$; hence, the uncertainty in the corrected conversion efficiency is in the order of $\pm 10\%$.

We define the output mode purity of the $LG_{3,3}$ SHG with respect to the $LG_{6,6}$ mode because it is expected to dominate the harmonic output field in an undisturbed situation [14]. We measured this purity with a CCD beam analyzer as done in Ref. [6].

The experimental setup (see Fig. 3) is designed for the usage of both the $LG_{0,0}$ and $LG_{3,3}$ mode and features a 2 W non-planar ring laser (NPRO) continuously emitting the $LG_{0,0}$ mode at a wavelength of 1064 nm. For downstream applications, two removable mirrors allow us to switch between the $LG_{0,0}$ mode and the conversion into the $LG_{3,3}$ mode performed by a diffractive optical element (DOE) with an efficiency of $75 \pm 5\%$ [6]. A set of quarter- and half-wave plates ensures a linear polarization in both beam paths. In transmission of the mode cleaner cavity (MC, finesse about 300, linewidth about 2.3 MHz), the mode purity of the $LG_{3,3}$ mode, measured with a WinCam, is at $98.7 \pm 0.3\%$. Its power transmission through DOE and MC is at about 45% when the MC is locked via the Pound–Drever–Hall (PDH) scheme. The subsequent combination of a half-wave plate and Faraday isolator (FI) allows for a tunable SHG input power, while the FI also provides the correct linear polarization (s-pol) for the SHG crystal and prevents any optical cross-talk between MC and SHG. $P_{in}^{ext}$ is measured with a portable powermeter in transmission of the electro-optical modulator (EOM), which operates at a frequency of 120 MHz (local oscillator, LO) for the SHG PDH lock. A beamsplitter (BS) reflects 99% of the light towards the SHG cavity and transmits 1% of the reflected light at 1064 nm towards the photo diode $PD_{refl}$. This PD provides the PDH error signal as well as a DC signal that is used to measure how much power is reflected in lock (to a good approximation, this is given by the ratio of the signal in lock to the maximum signal in the reflection spectrum during the length scan multiplied by $P_{in}^{ext}$). The dichroic BS (DBS) reflects all of the incoming light towards the SHG and transmits the harmonic field at 532 nm towards the powermeter $PD_{out}$. An additional PD in transmission of the SHG cavity measures the transmitted power/spectrum at 1064 nm (the transmitted harmonic power is negligibly small).

The SHG cavity (see Fig. 2) contains a 7% doped MgO:$LiNbO_3$ crystal, which measures $2.0 \times 2.5 \times 6.5$ mm in the $x$, $y$ and $z$ (propagation) directions. Its curved end face serves as a highly reflective end mirror: $R_{1064\,nm} > 99.96\%$ and $R_{532\,nm} = 99.9\%$. The nominal reflectivities of the incoupling mirror are $R_{1064\,nm} = 98.2\%$ and $R_{532\,nm} < 0.2\%$. The radii of curvature are $R_{c,in} = 25$ mm and $R_{c,end} = 12$ mm, setting the waist of the fundamental field to about 30 µm in radius near the crystal center. This corresponds to a focusing parameter of $\xi \approx 0.5$ [14]. The plane crystal face has an anti-reflective coating, and the SHG crystal temperature can be electronically stabilized via a control loop using a Peltier element as the actuator.

We measured the conversion efficiency of the $LG_{0,0}$ mode for an input power ranging from 2 mW to 370 mW. The external conversion efficiency (see Fig. 4) first steeply increased up to a maximum of $95.69 \pm 0.11\%$ at $P_{in}^{ext} \approx 80$ mW and then slowly decreased. This decrease is caused by the still rising internal conversion, which causes a transit of the impedance condition from over- to under-coupled around the maximum of the efficiency curve. Hence, the power buildup factor is reduced, and less circulating fundamental power is available for the SHG. The temperature setpoint of the crystal was adjusted over the range from 62.5°C to 62.1°C for maximal harmonic power at each data point. The mode matching was measured via the transmission spectrum to be $|\kappa|^2 = 97.5 \pm 1.5\%$, which puts the maximum of the corrected conversion efficiency to $98.7 \pm 1.5\%$ at $P_{in}^{mat} \approx 78$ mW. Since the harmonic output field showed no measurable deviation from a pure $LG_{0,0}$ mode, the output mode purity is set to $\mu_{out} = 1$, and the effective conversion efficiency is equal to the external one.

We measured the conversion efficiency of the $LG_{3,3}$ mode for an input power ranging from about 68 mW to 664 mW.

The external conversion efficiency rose up to a maximum of $45.1 \pm 0.2\%$, while the slope decreased. The optimum temperature setpoint for each data point was adjusted over the range from 62.1°C to 61.7°C. The flattening of the curve indicates an increase in astigmatism, which correlates with a decrasing $|\kappa|^2$ value (range from lowest to highest input power: $0.71 \pm 0.11 - 0.63 \pm 0.06$) and could also be observed with a CCD camera in the harmonic output field. Figure 4 shows the intensity distribution of the harmonic output field at 664 mW of input power with a harmonic power of about 300 mW. The mode purity in terms of the $LG_{6,6}$ mode was determined to be $\mu_{\mathrm{out}} = 64 \pm 5\%$. The same analysis was performed at an input power of about 131 mW; here, the mode purity was clearly higher at $\mu_{\mathrm{out}} = 71 \pm 5\%$. The increasing astigmatism can be explained by the increasing total absorption in the crystal, which influences its astigmatic effect on the circulating field via heating. Assuming a linear decrease in the output mode purity, Fig. 4 shows the effective conversion efficiency for all measurement points. It finally reaches $29 \pm 2\%$. The corrected conversion efficiency, derived with Eq. (5), reaches a maximum of $72 \pm 7\%$ at a matched input power of $P_{\mathrm{in}}^{\mathrm{mat}} = 420 \pm 40$ mW.

The NLCS simulation tool was used to calculate the harmonic power as a function of the matched input power with the cavity parameters of our experiment. For both the $LG_{0,0}$ and $LG_{3,3}$ case, the respective effective nonlinearity $d_{p,l}$ was used to optimize the match between measurement data and simulation. We derived $d_{0,0} = 2.6\ \mathrm{pm\ V^{-1}}$ and $d_{3,3} = 0.51\ \mathrm{pm\ V^{-1}}$. The simulations agree well with the measurement results.

In the SHG crystal, two "loss" coeffcients [1/m] act on the circulating fundamental power: the conversion and absorption coeffcient. But, while a rather small absorption coeffcient of the crystal can lead to a significant absorption loss due to the power buildup inside the cavity, this is typically not noticable in an $LG_{0,0}$ SHG due to the high conversion efficiency. Since the conversion efficiency of the $LG_{3,3}$ mode was, however, much lower in this experiment, the absorption loss was significant. For the $LG_{3,3}$ mode, the ratio of absorbed power to $P_{\mathrm{in}}^{\mathrm{ext}}$ started at about 10% and decreased to a final value of about 2% with increasing conversion efficiency. While this fractional loss was unexpectedly high, this is in good agreement with Eq. (5) and only requires a single-pass power loss coefficient $l^a$ in the order of $10^{-4}$, which is very similar to the roundtrip power loss in 7% doped MgO:$LiNbO_3$ measured in Ref. [20].

In conclusion, we have realized a cavity-enhanced SHG conversion efficiency of 95.7% in a 7% doped MgO : $LiNbO_3$ crystal for a fundamental input power of 80 mW in the $LG_{0,0}$ mode (cf., e.g., [21,22]). Furthermore, we could achieve a conversion efficiency of 45.1% for a fundamental input power of 664 mW in the $LG_{3,3}$ mode, mainly into the harmonic $LG_{6,6}$ mode. Such a high conversion efficiency has not been demonstrated with any higher-order mode before (cf. [23,24] for lower-order modes).

We showed that the $LG_{3,3}$ SHG is fundamentally less efficient than the $LG_{0,0}$ SHG and highly susceptible to astigmatism (see also [25]), which reduces both the conversion efficiency and the output mode purity. The derived ratio of the effective nonlinearities $d_{0,0}/d_{3,3} \sim 5$ implies that the $LG_{3,3}$ SHG requires about 25 times the input power of the $LG_{0,0}$ SHG for the same conversion efficiency assuming the same waist, perfect mode matching, equal absorption losses, and no astigmatism. With significant absorption of the $LG_{3,3}$ mode, it is rather in the order of 30. When comparing our measured values for the external and effective conversion efficiency, this factor is in the order of 100 and 700, respectively.

Since SHG and parametric down-conversion can be seen as reversed processes, the observed harmonic output field suggests that the generation of squeezed vacuum states in the $LG_{3,3}$ mode can only be efficiently pumped by the harmonic $LG_{6,6}$ mode in this focusing regime.

**Funding.** Deutsche Forschungsgemeinschaft (EXC-2123 QuantumFrontiers - 390837967).

**Disclosures.** The authors declare no conflicts of interest.

## REFERENCES


1. The LIGO Scientific Collaboration, Classical Quantum Gravity **32**,074001 (2015).
2. The Virgo Collaboration, Classical Quantum Gravity **32**, 024001 (2015).
3. J.-Y. Vinet, Classical Quantum Gravity **24**, 3897 (2007).
4. P. Fulda, K. Kokeyama, S. Chelkowski, and A. Freise, Phys. Rev. D **82**, 012002 (2010).
5. S. Chelkowski, S. Hild, and A. Freise, Phys. Rev. D **79**, 122002 (2009).
6. L. Carbone, C. Bogan, P. Fulda, A. Freise, and B. Willke, Phys. Rev. Lett. **110**, 251101 (2013).
7. A. Noack, C. Bogan, and B. Willke, Opt. Lett. **42**, 751 (2017).
8. A. Gatto, M. Tacca, F. Kéfélian, C. Buy, and M. Barsuglia, Phys. Rev. D **90**, 122011 (2014).
9. B. Sorazu, P. J. Fulda, B. W. Barr, A. S. Bell, C. Bond, L. Carbone, A. Freise, S. Hild, S. H. Huttner, J. Macarthur, and K. A. Strain, Classical Quantum Gravity **30**, 035004 (2013).
10. C. Bond, P. Fulda, L. Carbone, K. Kokeyama, and A. Freise, Phys. Rev. D **84**, 102002 (2011).
11. The Virgo Collaboration, Phys. Rev. Lett. **123**, 231108 (2019).
12. M. Mehmet and H. Vahlbruch, Classical Quantum Gravity **36**, 015014 (2019).
13. H. Vahlbruch, M. Mehmet, K. Danzmann, and R. Schnabel, Phys. Rev. Lett. **117**, 110801 (2016).
14. J. Heinze, H. Vahlbruch, and B. Willke, "Numerical analysis of $LG_{33}$ second harmonic generation in comparison to the $LG_{00}$ case," arXiv:2008.10243 (2020).
15. N. Lastzka, "Numerical modelling of classical and quantum effects in non-linear optical systems," Ph.D. thesis (Leibniz Universität Hannover, 2010).
16. T. D. Huang and T. H. Lu, Appl. Phys. B **124**, 72 (2018).
17. T. Hong, J. Miller, H. Yamamoto, Y. Chen, and R. Adhikari, Phys. Rev. D **84**, 102001 (2011).
18. K. Arai, "On the accumulated round-trip gouy phase shift for a general optical cavity," Technical Report LIGO-T1300189–v1 (LIGO Scientific Collaboration, 2013).
19. P. Kwee, F. Seifert, B. Willke, and K. Danzmann, Rev. Sci. Instrum. **78**, 073103 (2007).
20. H. Vahlbruch, M. Mehmet, S. Chelkowski, B. Hage, A. Franzen, N. Lastzka, S. Goßler, K. Danzmann, and R. Schnabel, Phys. Rev. Lett. **100**, 033602 (2008).
21. T. Südmeyer, Y. Imai, H. Masuda, N. Eguchi, M. Saito, and S. Kubota, Opt. Express **16**, 1546 (2008).
22. S. Ast, R. M. Nia, A. Schönbeck, N. Lastzka, J. Steinlechner, T. Eberle, M. Mehmet, S. Steinlechner, and R. Schnabel, Opt. Lett. **36**, 3467 (2011).
23. J. Courtial, K. Dholakia, L. Allen, and M. J. Padgett, Phys. Rev. A **56**, 4193 (1997).
24. Z.-Y. Zhou, Y. Li, D.-S. Ding, W. Zhang, S. Shi, B.-S. Shi, and G.-C. Guo, Opt. Express **22**, 23673 (2014).
25. A. Allocca, A. Gatto, M. Tacca, R. A. Day, M. Barsuglia, G. Pillant, C. Buy, and G. Vajente, Phys. Rev. D **92**, 102002 (2015).